Vacancy-suppressed lattice conductivity of high-ZT In_4Se_{3-x}

Hyo Seok Ji,[1] Hyoungchul Kim,[2] Changhoon Lee,[1] Jong-Soo Rhyee,[3] Moo Hwan Kim,[4] Massoud Kaviany,[2,4] and Ji Hoon Shim[1,4,5,*]

[1]*Department of Chemistry, Pohang University of Science and Technology, Pohang 790-784, Korea*
[2]*Department of Mechanical Engineering, University of Michigan, Ann Arbor, Michigan 48109-2125, USA*
[3]*Department of Applied Physics, Kyung Hee University, Yongin 446-701, Korea*
[4]*Division of Advanced Nuclear Engineering, Pohang University of Science and Technology, Pohang 790-784, Korea*
[5]*Department of Physics, Pohang University of Science and Technology, Pohang 790-784, Korea*

(Received 24 December 2012; published 8 March 2013)

Anomalous, vacancy-induced anisotropic thermal conductivity is one of the important properties in the recently discovered high-ZT In_4Se_{3-x} compound. In this work, the lattice thermal conductivity of In_4Se_{3-x} is investigated using equilibrium molecular dynamics simulation, the point-defect model, and *ab initio* calculations. The charge density distribution shows highly anisotropic structure with strong bonding along In-Se-In chain direction. Se vacancy strongly suppresses the phonon propagation along the chain direction, with little change in other directions. We show that suppressed long-range acoustic phonon transport caused by the vacancy results in anisotropic change of lattice conductivity. We suggest controlling of vacancy in intrinsic low-dimensional compounds is critical in achieving optimal lattice thermal conductivity and other thermoelectric properties.

DOI: 10.1103/PhysRevB.87.125111 PACS number(s): 72.20.Pa, 66.70.Df, 63.20.Ry

I. INTRODUCTION

The n-type semiconductor In_4Se_{3-x} was reported to be a good thermoelectric (TE) material.[1] The TE figure of merit $ZT = S^2\sigma_e T/(k_e + k_p)$ (S, σ_e, T, k_e, and k_p are the Seebeck coefficient, electrical conductivity, absolute temperature, and electric and lattice thermal conductivities, respectively) is 1.48 at 705 K for $In_4Se_{2.35}$ (which is currently the highest among n-type bulk semiconductors). The charge density wave (CDW) induced by quasi-one-dimensional lattice distortion (Peierls distortion) enhances the power factor $S^2\sigma_e$ and lowers lattice conductivity.[1] This suggests a different direction in the search for high-ZT TE materials, beyond Bi_2Te_3 and PbTe. Recently, experiments using chemical doping[2–4] and nanostructures[5] have aimed at further increasing ZT of In_4Se_{3-x}, and there has been theoretical investigation of high-ZT In_4Se_{3-x} using the electronic structure calculations.[6]

The electronic properties such as S and σ_e of In_4Se_{3-x} are well investigated by the combination of Boltzmann transport equation and *ab initio* band structure calculations.[1] Using a simple rigid-band and constant relaxation time approximation, the calculated power factor is in good agreement with the experimental results. Also the electronic structure calculation predicts the enhancement of the power factor with electron doping, which is correctly realized in Cl-doped structure ($In_4Se_{3-x}Cl_{0.03}$).[2] Thermal conductivity, however, is not well described by electronic structure calculations because the lattice (phonon) contribution is dominant over electric thermal conductivity.[2] For accurate prediction of ZT in In_4Se_{3-x}, the lattice dynamics and phonon scattering should be investigated.

The orthorhombic lattice structure (space group $Pnnm$) of In_4Se_3 contains warped b-c plane layers which are stacked along the a axis [Fig. 1(a)]. Within the layer, three distinction In-Se-In zigzag chains are aligned along the c axis [Fig. 1(b), indicated by black, blue, and red lines]. For all the chains, the In atoms are connected with Se atoms by an ionic-covalent bond. The warped layers are stacked with a weak intermolecular bond along the a direction.[7] Most of the layered compounds usually show higher in-plane thermal conductivity than that of the cross plane because of the strong interatomic bonding. However, experimental thermal conductivity of In_4Se_{3-x} shows unusual behavior; the b-c plane thermal conductivity is much lower than that in the a-b plane.[1] Because high In_4Se_{3-x} ZT is closely related to the low b-c plane thermal conductivity, it will be important to explain this unusual anisotropy in the lattice thermal conductivity.

The high-temperature lattice conductivity of semiconductors has been explained with the simple analytical approach, point-defect model, developed by Klemens[8] and Callaway and von Baeyer.[9] This model, derived from the consideration of phonon scattering processes to the thermal resistance, has been successfully applied to thermal transport in a variety of TE materials.[10–14] Various crystal imperfections (e.g., vacancies, interstitial atoms, and site substitution) can be considered as point defects to reduce the lattice conductivity due to the phonon scatterings with mass contrast, atomic displacement, and/or local strain induced by the defect. In In_4Se_{3-x}, the randomly distributed Se vacancies are expected to scatter phonons. However, the point-defect model has not commonly applied to a highly anisotropic system such as In_4Se_{3-x}.

Here using molecular dynamics (MD) simulation, the point-defect model, and *ab initio* calculations, we investigate the lattice conductivity of In_4Se_{3-x} crystal to (i) predict the lattice conductivity tensor of In_4Se_{3-x} and (ii) explain the origin of its unusual anisotropy. Our results show the lattice conductivity along the chain direction is sensitively suppressed with the Se-deficient In_4Se_{3-x} structure. On the other hand, the Se vacancy moderately suppresses the lattice conductivity perpendicular to the chain. So the low in-plane (b-c plane) lattice conductivity in In_4Se_{3-x} is consistent with the experimental observations.

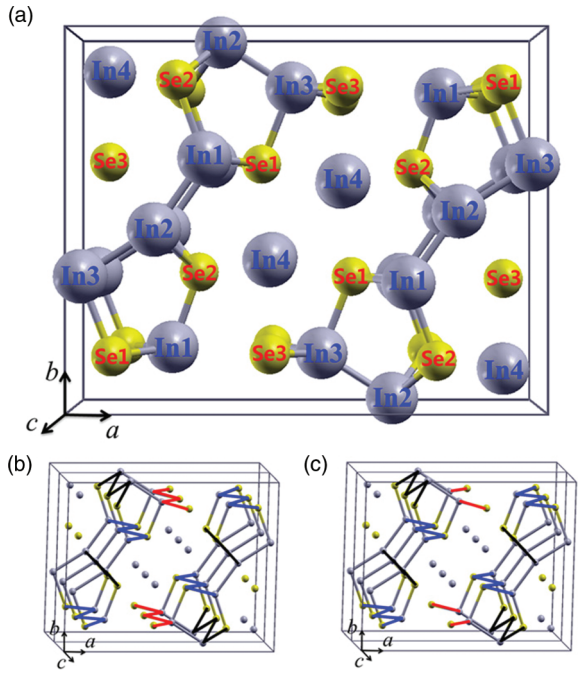

FIG. 1. (Color online) Crystal structure of In_4Se_3. (a) Perspective view of the a-b plane. Gray and yellow spheres represent In and Se atoms, respectively. (b) The structure contains three distinct In-Se-In chains along the c axis; blue, black, and red lines indicate In1-Se1, In2-Se2, and In3-Se3 chains, respectively. (c) Crystal structure of In_4Se_{3-x}, containing Se3 vacancy.

II. METHODS AND MODELS

A. *Ab initio* calculations

In order to determine the preference of Se vacancy sites in In_4Se_3, we construct a hypothetical crystal structure and remove one Se atom of In_4Se_3 at the Se1, or Se2, or Se3 sites, respectively. In our density functional calculations of In_4Se_3, we employed the frozen-core projector augmented wave method[15,16] encoded in the Vienna *ab initio* simulation package,[17] and the generalized-gradient approximation of Perdew, Burke, and Ernzerhof[18] for the exchange-correlation functional with the plane-wave-cutoff energy of 450 eV and a set of 80 κ points in the irreducible Brillouin zone. The threshold for the self-consistent-field convergence of the total electronic energy was 10^{-6} eV.

B. Interatomic potentials

We construct the classical interatomic potentials for In_4Se_3 developed on the basis of experimental lattice properties by using GULP (general utility lattice program).[19] The classical Morse and three-cosine interatomic potentials were fitted to the elastic constants. The fitted interatomic potentials undergo the GULP optimization of the crystal structure under constant pressure. In the fitting process, we calculate the elastic constants C_{ij} and then compare them with the experimental values.[20] The resulting C_{ij} are listed in Table I and compared with the experiments. Our results show better agreement with experiments than those in the previous theoretical results[7] with only central two-body interactions.[7] The resulting optimized potential parameters are listed in Table II.

C. Lattice conductivity from MD simulations

The high-temperature ($T > 0.1T_D$, where T_D is the Debye temperature) lattice conductivity tensor $\mathbf{K}_p$ is dominated by phonon-phonon scattering and is calculated using equilibrium MD and the Green-Kubo heat current autocorrelation function (HCACF) decay,[21,22]

$$\mathbf{K}_p = \frac{V}{k_B T^2}\int_0^\infty \langle \mathbf{q}(t)\mathbf{q}(0)\rangle, \tag{1}$$

where k_B is the Boltzmann constant, V is the volume of the MD simulation, $\langle \mathbf{q}(t)\mathbf{q}(0)\rangle$ is the HCACF tensor, and the heat current vector $\mathbf{q}$ is

$$\mathbf{q} = \frac{1}{V}\frac{d}{dt}\sum_{i=1}^{N}\mathbf{r}_i E_i, \tag{2}$$

where $\mathbf{r}$ and E are the position vector and the total energy of the particle (atom), respectively. After checking the size effect on the result of MD simulation, the simulations are performed in $3 \times 3 \times 12$ orthorhombic unit cells with 3024 (3024–432x for In_4Se_{3-x}) atoms. The temperature ranges from 300 to 700 K, with 100 K interval with a time step of 20 fs. The Verlet leapfrog algorithm with the Nose-Hoover thermostat and the Berendsen barostat are used in the *NPT* ensemble for 200 ps and then in *NVE* for 100 ps to reach equilibrium. Then 2000 ps raw heat current data are obtained for the calculation of HCACF. The resulting HCACF is then directly integrated and $\mathbf{K}_p$ is averaged in the smoothened converged region.

D. Point-defect model of lattice conductivity

In order to analyze the change of $\mathbf{K}_p$ as a function of Se vacancy concentration (x) and temperature, we use the analytical treatment, point-defect model. Starting with $\mathbf{K}_p$ of In_4Se_3 ($x = 0$), which are dominated by the phonon-phonon scattering, we add the point-defect scattering for the compound with vacancies.

From the Matthiessen rule, the isotropic overall $k_{p,x}$ with the inclusion of the point-defect scattering $k_{p,d}$ is $1/k_{p,x}(T) = 1/k_{p,0}(T) + 1/k_{p,d}(T)$. Here $k_{p,0}(T)$ is obtained from our MD results. For the description of $k_{p,d}$, we start with the mass

TABLE I. Comparison of calculated elastic constants C_{ij} (in GPa) of In_4Se_3 compared with experiments and other theoretical results.

	C_{11}	C_{12}	C_{13}	C_{22}	C_{23}	C_{33}	C_{44}	C_{55}	C_{66}
Experiment[20]	38.2	10.8	30.4	66.5	22.4	64.3	16.6	26.6	19.0
Other theoretical results[7]	49.8	15.6	26.1	58.9	21.7	52.2	18.7	33.0	16.1
This study	36.4	13.7	22.4	68.9	24.9	62.0	20.5	32.5	22.7

TABLE II. The two- and three-body interatomic potential parameters (excluding the electrostatic interactions) for In_4Se_3. Morse potential $\varphi_o\{[1-\exp(-a(r-r_o))]^2-1\}$ for two-body and three cosine $[\varphi_\theta(\cos\theta-\cos\theta_o)^2]/2$ for three-body interactions. Here, r and θ are interatomic separation distance and bond angle.

Interaction	Parameters			Interaction	Parameters	
Two-body	φ_o (eV)	a (Å^{-1})	r_o (Å)	Three-body	φ_θ (eV)	θ_o (deg)
In1-Se1	1.83	1.67	2.69	Se1-In1-Se1	1.44	98.6
In2-Se2			2.80	Se2-In2-Se2		93.6
In3-Se3			2.63	Se3-In3-Se3		101.5
In1-Se2	1.29	1.27	2.62	In1-Se1-In1	1.44	98.6
In3-Se1			2.71	In2-Se2-In2		93.6
In2-In3	1.44	1.32	2.75	In3-Se3-In3		101.5
In1-In2			2.78	In3-In2-In1	1.82	157.8
In2-Se3	0.96	1.19	3.43	Se2-In2-In1		98.5
In3-In3			3.69	In2-In1-Se2		125.1
In4-In4	0.9	1.3	3.44	Se1-In1-In2		109.7
In4-In2			3.79	Se1-In3-Se3	1.94	100.2
In4-Se3	0.7	0.45	2.97	In2-In3-Se3		124.1
In4-Se2	0.6	1.01	3.16	Se2-In2-In3	1.91	96.7
In4-Se1	0.5	1.03	3.39	Se1-In1-Se2		105.2
In4-Se1	0.4	1.0	3.74	In1-Se1-In3		101.1
				Se1-In3-In2		101.3
				In2-Se2-In1		108.7

fluctuation scattering parameter Γ, which is given by

$$\Gamma = x(1-x)\left[\left(\frac{\Delta M}{M}\right)^2\right], \tag{3}$$

where M is the average mass of compound In_4Se_{3-x}. The lattice conductivity limited by the point-defect scattering $k_{p,d}$ is

$$k_{p,d} = \frac{k_B}{4\pi u_{p,A}(a_1 CT)^{1/2}}, \tag{4}$$

where k_B is the Boltzmann constant, CT is the relaxation time for interphonon scattering including normal (N) and umklapp (U) processes. Here CT can be estimated from the pure In_4Se_3 at 300 K using

$$CT = \frac{(6n)^{1/3}k_B}{2\pi^{4/3}k_{p,0}}, \tag{5}$$

where n is the atomic number density. The parameter a_1 is the coefficient for the Rayleigh point-defect scattering rate, given by

$$a_1 = \frac{V_c\Gamma}{4\pi u^3_{p,g,A}}, \tag{6}$$

where V_c is the unit-cell volume and $u_{p,g,A}$ is the average phonon group velocity.

III. RESULTS AND DISCUSSION

A. Se vacancy formation

Table III shows the relative energy of each Se vacancy model obtained from *ab initio* calculations, and shows that Se3 is the most preferable site for the formation of the Se vacancy. The result is reasonable considering the bonding structures around the Se ions. As shown in Fig. 1(a), Se3 has only two nearest neighbors, while Se1 and Se2 have three nearest neighbors with ionic-covalent bonding with In atoms. Because Se1 and Se2 are very important in sustaining stable *b*-*c* plane layer, the Se3 is the most probable vacancy site. So in the MD simulations, we use only Se3 vacancy for In_4Se_{3-x} structure. To avoid the repetition of the Se3 vacancies along the *c* direction, we use a $1\times1\times4$ supercell to distribute the Se3 vacancies randomly. We also considered several other structure orders with different Se3 vacancy sites and the results showed consistent anisotropic behavior of the lattice conductivity. To fully examine all possible Se3 sites, a much larger supercell is required (computation is very extensive) and that was considered outside the scope of the current study.

B. Lattice conductivity of In_4Se_{3-x}

Our equilibrium MD based lattice conductivity results for In_4Se_3 show the expected temperature dependence as shown in Fig. 2(a). For $x=0$, the *c*-direction lattice conductivity is much larger than that in other directions for all temperatures. This makes the *b*-*c* plane lattice conductivity larger than the *a*-*b* plane, which we expect from the lattice and elastic constants. For $x=0.5$, however, the *c*-direction lattice conductivity is noticeably reduced, while the *a*- and *b*-direction lattice conductivity show much smaller suppression [Fig. 2(a), dashed lines]. In Fig. 2(a), we remove standard error bars because of complexity, which is allowed in the 10%–20% range. The error is decreased as temperature and Se vacancy increases. Our results are well consistent with the experimental observation[1]

TABLE III. Relative energy of Se vacancy atom (with respect to Se3) sites in the structure model.

Site	Se1	Se2	Se3
ΔE (meV)	131.92	65.20	0.00

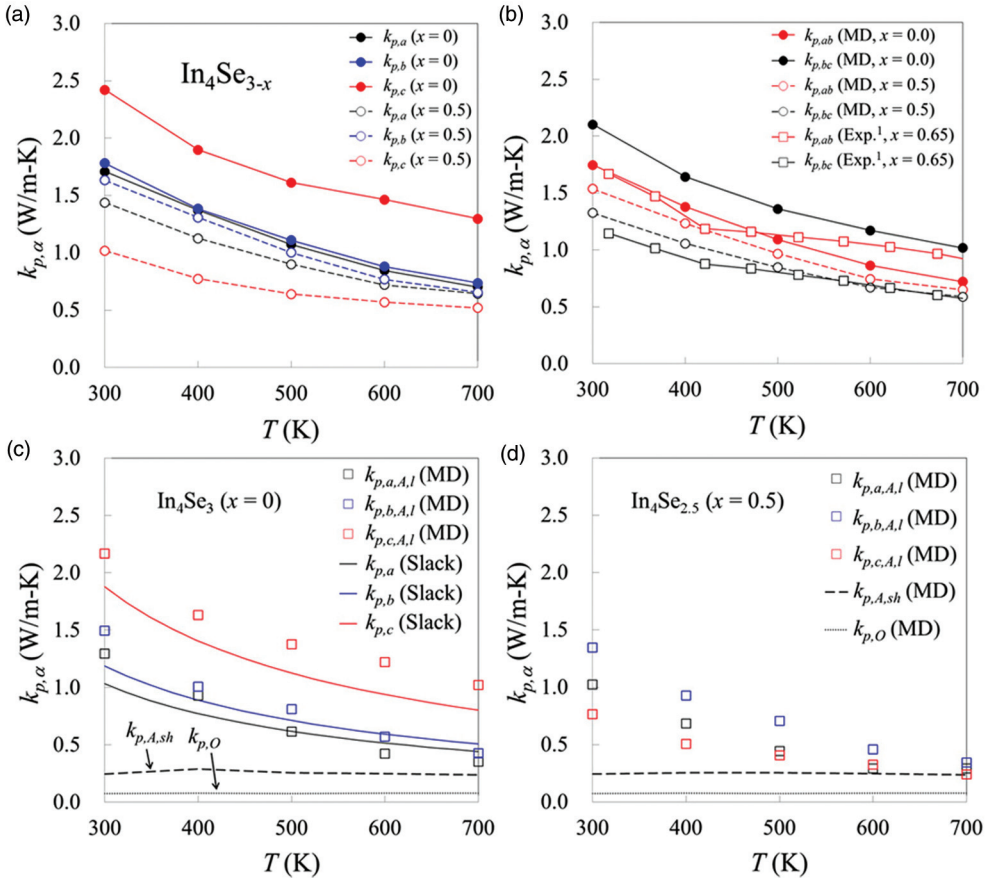

FIG. 2. (Color online) (a) Variation of the directional lattice conductivity as a function of temperature for In_4Se_3 ($x = 0$, solid lines) and $In_4Se_{2.5}$ ($x = 0.5$, dashed lines). (b) The calculated a-b and b-c plane lattice conductivities and comparison to experiment.[1] (c) The decomposition of lattice conductivity and comparison to the Slack relation for In_4Se_3 ($x = 0$). (d) The decomposition of lattice conductivity for $In_4Se_{2.5}$ ($x = 0.5$).

that the a-b plane thermal conductivity is larger than the b-c plane thermal conductivity in $In_4Se_{2.35}$ [Fig. 2(b)].

In order to understand the mechanism of thermal transport, we decomposed the lattice conductivity of In_4Se_{3-x} into three components: short-range acoustic, long-range acoustic, and optical[23,24]

$$k_p = \frac{1}{k_B V T^2}\left(A_{A,sh}\tau_{A,sh} + A_{A,lg}\tau_{A,lg} + \sum_i \frac{B_{i,O}\tau_{i,O}}{1+\tau_{i,O}^2}\right) = k_{p,A,sh} + k_{p,A,lg} + k_{p,O}, \quad (7)$$

where τ_i is the time constant, A_i and B_i are constants, and the subscripts sh, lg, A, and O refer to short-range, long-range, acoustic, and optical. First, the optical component of HCACF is filtered by fast Fourier transform with a cutoff frequency of 1.5 THz. Then the acoustic component is fitted with two exponential functions, i.e., a fast decaying short-range and a slow decaying long-range decay.[14,21,22] The long-range acoustic lattice conductivity has a strong temperature dependence [Fig. 2(c), rectangular symbol] and dominates the lattice conductivity, while the short-range acoustic and optical lattice conductivities are relatively small and independent of temperature and direction (i.e., $k_{p,A,sh} = 0.25$ and $k_{p,O} = 0.08$ W/m K). For $In_4Se_{2.5}$ ($x = 0.5$), this phonon transport decomposition shows suppression of the long-range acoustic transport mainly, while the temperature-independent, short-range acoustic, and optical transports remain almost the same [Fig. 2(d)]. So we confirmed only the long-range acoustic phonon is suppressed with Se vacancy, which will be discussed later.

TABLE IV. Calculated directional Debye temperatures, Grüneisen parameters, and average phonon group velocities of In_4Se_{3-x}. An available Debye temperature is also listed.

Directions (α)	$T_{D,\alpha}$ (K)	$\gamma_{G,\alpha}$	$u_{p,g,A,\alpha}$ (m/s, $x = 0$)	$u_{p,g,A,\alpha}$ (m/s, $x = 0.25$)	$u_{p,g,A,\alpha}$ (m/s, $x = 0.5$)
a	226	1.94	2286	2186	2029
b	226	1.81	2287	2239	2183
c	239	1.56	2311	2145	1922
Ref. 3	260				

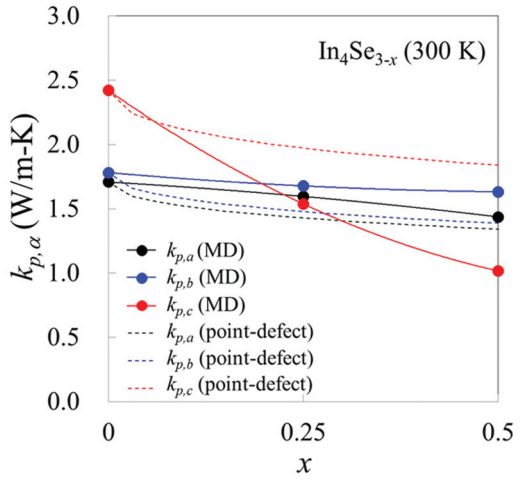

FIG. 3. (Color online) Variation of the directional lattice conductivity of In_4Se_{3-x} as a function of vacancy at 300 K. The calculated MD results (solid lines) are compared with the point-defect model (dashed lines).

To verify our MD lattice conductivity we compare it with the directional Slack relation which represent the long-range phonon conductivity,[25,26] i.e.,

$$k_{p,\mathrm{S},\alpha} = \frac{3.1 \times 10^4 \langle M \rangle N_c^{1/3} \delta T_{\mathrm{D},\infty,\alpha}^3}{T \gamma_{G,\alpha}^2}, \ \alpha = a,b, \text{ or } c. \tag{8}$$

Here, $\langle M \rangle$ is the mean atomic weight of the atoms in the primitive cell, δ is the average volume per atom, N_c is the number of atoms in a primitive cell, $T_{\mathrm{D},\infty}$ is the high-temperature Debye temperature, and $\gamma_{G,\alpha}$ is the directional Grüneisen parameter (indicative of the bonding character in the lattice[26]) defined as

$$\gamma_{G,\alpha} = -\sum_{\kappa} \frac{d \ln \omega_\alpha(\kappa)}{d \ln V}, \tag{9}$$

where $\omega_\alpha(\kappa)$ is phonon frequency. Directional Debye temperature and Grüneisen parameter, which are obtained from the MD results using the interatomic potentials, are listed in Table IV. Due to the strong bond along the c direction, $\gamma_{\mathrm{G},c}$ has the lowest value. Using these results, the directional long-range acoustic lattice conductivity calculated by Eq. (8) is also shown in Fig. 2(c). The directional Slack results are in reasonable agreement with the decomposed MD results for In_4Se_3 ($x = 0$).

C. Anisotropic reduction in lattice conductivity of In_4Se_{3-x}

To investigate the unusual anisotropic behavior of In_4Se_{3-x}, we compare directional lattice conductivities with respect to Se vacancy x in Fig. 3 at 300 K. For In_4Se_3 ($x = 0$), the c-direction lattice conductivity is the largest, which makes the b-c plane conductivity larger than that in the a-b plane. With Se vacancy, the c-direction conductivity is reduced a lot more compared to a and b directions. For $In_4Se_{2.5}$ ($x = 0.5$), the c-direction conductivity is smaller compared to a and b directions, as already shown in Fig. 2.

We also analyzed the effect of Se vacancy with the point-defect model. For calculation of the lattice conductivity with Eq. (4), we use the reported and calculated thermodynamic/phonon properties at room temperature summarized in Table IV. These analytical model results for the point-defect scattering model are compared with the MD results in Fig. 3. The model predictions along the a and b direction are in good agreement with the MD results over the range of vacancy concentration and temperature. Hence we conclude that the isotropic point-defect scattering including the mass fluctuation accurately predicts the $\mathbf{K}_p$ reduction in In_4Se_{3-x} in these directions. Along the c direction, however, the isotropic point-defect model does not predict the significant suppression of $k_{p,\alpha}$, suggesting the phonon softening due to the bond softening is significantly directional in this material. This anisotropy results in an extra 50% reduction of $k_{p,\alpha}$ over what is predicted by the isotropic point-defect model.

D. Origin of vacancy-induced anisotropy in lattice conductivity

To explain the origin of the anisotropic effect of vacancy on the lattice conductivity, we calculate the phonon dispersion curves for In_4Se_{3-x} using the obtained interatomic potentials. Figure 4(a) shows the total phonon dispersion for each direction in the In_4Se_3 structure. The dispersion is well matched with that reported in Ref. 7. With Se vacancy [Fig. 4(b)], a flat dispersion curve around 1 THz appears to contribute to

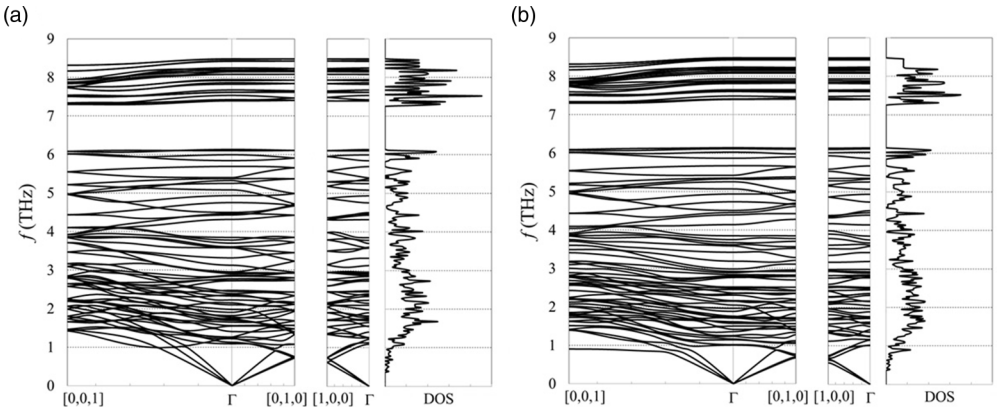

FIG. 4. Phonon dispersion curves and density of state of (a) In_4Se_3 and (b) $In_4Se_{2.75}$. [1,0,0], [0,1,0], and [0,0,1] indicate the a-, b-, and c-directions in the structure, respectively.

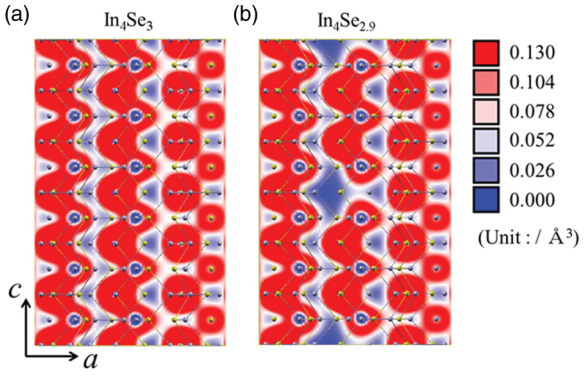

FIG. 5. (Color online) Charge density distributions in the (a) In_4Se_3 and (b) $In_4Se_{2.9}$ lattice.

the acoustic phonon dispersion along the c direction. Along a and b directions, there is negligible change in the acoustic phonon dispersion. As a result, the phonon velocity along the c direction is significantly suppressed with the Se vacancy, while other directions are showing small changes. Because the point-defect model considered generally uses the no-defect phonon velocities, the a- and b-direction conductivities are well described by the point-defect model. However, the c-direction conductivity is suppressed more than that predicted by the point-defect model. The changes in the phonon velocity with the Se vacancy along each direction are summarized in Table IV. While the phonon velocity for a and b directions decrease by 11% and 5% for $x = 0.5$, the c direction shows 17%.

The suppressed phonon velocity along the c direction can be understood with the crystal structure containing the In-Se-In chains along c direction, as shown in the Fig. 1(b). The bundle of atomic chains along the c direction makes for high lattice conductivity because of high phonon speed along that direction in the absence of vacancy. The bondings along a and b directions have more complicated structures compared with the c direction. With Se vacancy, the conducting channels of In-Se-In chains are broken. The chain breaking is well described by the charge density distributions in In_4Se_3 and $In_4Se_{2.9}$ lattice as shown in Figs. 5(a) and 5(b). In Fig. 5(a), the charge density distribution shows strong bonding along In-Se-In chains, which give high phonon transport of the In_4Se_3 compound. When the strong In-Se-In bonding is broken [Fig. 5(b)], the disconnected charge density reduces phonon transport, especially along the c.

Also, the CDW induced structural distortion, which is argued in Ref. 1, could break the quasi-one-dimensional chains to suppress the phonon transport. So the In-Se-In chain and the vacancy in the chain are the key elements to explain the anisotropic lattice conductivity in the In_4Se_{3-x} compound.

IV. CONCLUSIONS

In summary, we investigated the anisotropic behavior of lattice conductivity for the In_4Se_{3-x} compound using various theoretical works. The interatomic potentials are developed for MD simulation and lattice conductivity prediction of In_4Se_{3-x}, and the good agreement of the calculated elastic constants with the experiments indicates that the proposed force fields are suitable for both harmonic and anharmonic behaviors of In_4Se_3. Using developed interatomic potential, the temperature dependence of directional lattice conductivities has been calculated in a temperature range from 300 to 700 K with and without Se vacancy. The results reproduce well the experimental observations of lattice conductivities with Se vacancy. Without Se vacancy, c-direction conductivity is the highest due to strong bonding along In-Se-In chain, while it is suppressed even below a- and b-direction conductivity with Se vacancy. The calculated phonon dispersion and the charge density distribution also support the anisotropic changes of lattice conductivity.

We show that the Se vacancy in the quasi-one-dimensional In-Se-In chain has a dominant role in the suppression of long-range acoustic phonon transport and very low lattice conductivity along the chain direction. Our results could give a different direction for finding good TE materials in controlling the lattice conductivity.

ACKNOWLEDGMENTS

Work at Pohang University of Science and Technology was supported by the National Research Foundation of Korea (NRF) funded by the Ministry of Education, Science and Technology (Grants No. 20110030147 and No. R32-2008-000-10180-0). Work at Kyung Hee University was supported by Basic Science Research Program through NRF (Grants No. 2011-0021335 and No. 2012R1A2A1A03005174). Work at the University of Michigan was supported by the Center for Solar and Thermal Energy Conversion, an Energy Frontier Research Center funded by the U.S. Department of Energy, Office of Science, Office of Basic Energy Science under Award No. DE-SC-0000957.

*Corresponding author: jhshim@postech.ac.kr

[1] J. S. Rhyee, K. H. Lee, S. M. Lee, E. Cho, S. I. Kim, E. Lee, Y. S. Kwon, J. H. Shim and G. Kotliar, Nature (London) **459**, 965 (2009).
[2] J. S. Rhyee, K. Ahn, K. H. Lee, H. S. Ji, and J. H. Shim, Adv. Mater. **23**, 2191 (2011).
[3] K. Ahn, E. Cho, J.-S. Rhyee, S. I. Kim, S. M. Lee, and K. H. Lee, Appl. Phys. Lett. **99**, 102110 (2011).
[4] K. Ahn, E. Cho, J.-S. Rhyee, S. I. Kim, S. Hwang, H.-S. Kim, S. M. Lee, and K. H. Lee, J. Mater. Chem. **22**, 5730 (2012).
[5] G. H. Zhu, Y. C. Lan, H. Wang, G. Joshi, Q. Hao, G. Chen, and Z. F. Ren, Phys. Rev. B **83**, 115201 (2011).
[6] L. Makinistian, E. A. Albanesi, N. V. Gonzalez Lemus, A. G. Petukhov, D. Schmidt, E. Schubert, M. Schubert, Ya. B. Losovyj, P. Galiy, and P. Dowben, Phys. Rev. B **81**, 075217 (2010).
[7] D. M. Bercha, K. Z. Rushchanskii, and M. Sznajder, Phys. Status Solidi B **212**, 247 (1999).
[8] P. G. Klemens, Phys. Rev. **119**, 507 (1960).
[9] J. Callaway and H. C. von Baeyer, Phys. Rev. **120**, 1149 (1960).

[10]G. P. Meisner, D. T. Morelli, S. Hu, J. Yang, and C. Uher, Phys. Rev. Lett. **80**, 3551 (1998).
[11]G. S. Nolas, J. L. Cohn, and G. A. Slack, Phys. Rev. B **58**, 164 (1998).
[12]Č. Drašar, M. Steinhart, P. Lošták, H.-K. Shin, J. S. Dyck, and C. Uher, J. Solid State Chem. **178**, 1301 (2005).
[13]B. Huang and M. Kaviany, Acta Mater. **58**, 4516 (2010).
[14]H. Kim, M. Kaviany, J. C. Thomas, A. Van der Ven, C. Uher, and B. Huang, Phys. Rev. Lett. **105**, 265901 (2010).
[15]P. E. Blöchl, Phys. Rev. B **50**, 17953 (1994).
[16]G. Kresse and D. Joubert, Phys. Rev. B **59**, 1758 (1999).
[17]G. Kresse and J. Furthmüller, Phys. Rev. B **54**, 11169 (1996).
[18]J. P. Perdew, K. Burke, and M. Ernzerhof, Phys. Rev. Lett. **77**, 3865 (1996).
[19]J. D. Gale and A. L. Rohl, Mol. Simul. **29**, 291 (2003).
[20]V. Ya. Kuriachii, V. Yu. Bogachev, V. P. Mikhalchenko, and I. M. Stakhira, Izv. Akad. Nauk SSSR, Ser. Neorg. Mater. **22**, 855 (1986).
[21]M. Kaviany, *Heat Transfer Physics* (Cambridge University Press, New York, 2008).
[22]B. L. Huang and M. Kaviany, Phys. Rev. B **77**, 125209 (2008).
[23]A. J. H. McGaughey and M. Kaviany, Int. J. Heat Mass Transf. **47**, 1799 (2004).
[24]B. L. Huang, A. J. H. McGaughey, and M. Kaviany, Int. J. Heat Mass Transf. **50**, 393 (2007).
[25]G. A. Slack, Solid State Phys. **34**, 1 (1979).
[26]B. L. Huang and M. Kaviany, J. Appl. Phys. **100**, 123507 (2006).